

Physical limitations to efficient high-speed spin-torque switching in magnetic tunnel junctions

R. Heindl,* W. H. Rippard, S. E. Russek, and A. B. Kos

National Institute of Standards and Technology, Boulder, Colorado 80305, USA

(Received 1 November 2010; revised manuscript received 4 January 2011; published 24 February 2011)

We have investigated the physical limitations to efficient high-speed spin-torque switching by means of write error rates both experimentally as well as through macrospin simulations. The spin-torque-induced write operations were performed on in-plane MgO magnetic tunnel junctions. The write error rates were determined from up to 10^6 switching events as a function of pulse amplitude and duration (5 to 100 ns) for devices with different thermal stability factors. Both experiments and simulations show qualitatively similar results. In particular, the write error rates as a function of pulse voltage amplitude increase at higher rates for pulse durations below ≈ 50 ns. Simulations show that the write error rates can be reduced only to some extent by the use of materials with perpendicular anisotropy and reduced damping, whereas noncollinear orientation of the spin current polarization and the magnetic easy axis increases the write error rates. The cause for the write error rates is related to the underlying physics of spin-torque switching and the occurrence of the stagnation point on the magnetization switching trajectory where the spin-torque disappears and the device loses the energy needed to switch. The stagnation point can be accessed either during the initial magnetization distribution or by thermal diffusion during the switching process.

DOI: [10.1103/PhysRevB.83.054430](https://doi.org/10.1103/PhysRevB.83.054430)

PACS number(s): 75.76.+j, 85.75.Dd

I. INTRODUCTION

Spin-transfer-torque^{1,2} random access memory (STT-RAM) based on MgO magnetic tunnel junctions (MTJ) is of great interest for nonvolatile memory applications.^{3,4} Significant progress has been made recently in the development of MgO MTJ's suitable for STT-RAM devices, and there are predictions that STT-RAM can be scaled down to the 22-nm node.⁵⁻⁷ For a functional device, however, many parameters are important, among which is the ability to reliably switch the magnetization by means of short (nanosecond) voltage pulses.⁸ The probability that the magnetization does not switch in response to an applied voltage (current) pulse that is expected to switch the magnetization at $V > V_{c0}$ ($I > I_{c0}$) (Ref. 9) is commonly referred to as the write error rate (WER).^{10,11} The prediction is that a tolerable WER should be $1.5 \times 10^{-7} - 6 \times 10^{-10}$ depending on the error correction code,^{7,12} subject to the constraint that the switching voltage at a particular WER has to be well below the lowest value of the tunnel junction breakdown voltage V_{bd} (≈ 1 V) (Refs. 13–15). To make STT-RAM compatible with the scaling of complementary metal-oxide semiconductor technology, the intrinsic switching current density ($I_{c0}/area$) needs to be reduced to below 2×10^6 A/cm², while keeping the thermal stability ($\Delta = E_{\text{barrier}}/k_B T$) (Ref. 16) above the value of 40 for data retention times of ten years.⁴ As we discuss below, for simple in-plane magnetized devices, achieving such low WER within these constraints is hampered by the existence of a “stagnation point” during the switching process where the switching energy is suddenly lost.

The intrinsic switching current of in-plane STT-RAM is proportional to¹⁷

$$I_{c0} \propto \frac{\alpha M_s}{\cos(\phi) P} (H_k^x + H_{k\text{-eff}}^z), \quad (1)$$

where α is the material dependent damping, M_s is the free layer saturation magnetization, ϕ is the in-plane angle between the spin-current polarization and the free-layer easy axis, P is

the spin-current polarization, H_k^x is the free-layer in-plane anisotropy field, $H_{k\text{-eff}}^z$ is the free layer effective out-of-plane demagnetization field ($H_{k\text{-eff}}^z = H_d^z - H_k^z$), H_d^z is the free-layer out-of-plane demagnetization field, and H_k^z is the free layer out-of-plane anisotropy. The in-plane anisotropy field arises predominantly from bit shape and is usually much smaller than the out-of-plane anisotropy, which is due to either surface or crystalline anisotropies. Thus I_{c0} can be manipulated by changing α , M_s , P , or the in-plane polarization angle ϕ , or by introducing perpendicular anisotropy H_k^z , while keeping M_s in-plane.¹⁸ In this paper, we present measurements of the WER of in-plane MgO MTJ's by attempting to switch the device state 10^6 times at various voltage pulses and durations, and compare our experimental results with macrospin simulations. We also determine the dependence of the WER on the parameters mentioned above that influence the switching current: Δ , α , H_k^z , and in- and out-of-plane polarization angles ϕ , θ . We did not study how P and M_s affect the WER since P is already assumed to be high (we use $P = 0.8$ in the simulations), and changing M_s affects the value of Δ , which complicates the analysis.

II. EXPERIMENTAL RESULTS

Our experimental setup consists of a 10 GS/s arbitrary function generator, a nanoscale MgO MTJ embedded into a coplanar waveguide structure, and a 13 GHz digital storage oscilloscope.¹⁹ The devices were processed from a starting thin-film stack:²⁰ 5 Ta/15 PtMn/2.3 Co₇₀Fe₃₀/0.8 Ru/2.5 Co₄₀Fe₂₀B₄₀/0.87 MgO/1.5 Co₄₀Fe₄₀B₂₀/10 Ta/7 Ru (thickness in nm). We performed experiments on numerous devices, but for clarity we present here data from only three devices. The devices are elliptical nanopillars of dimensions 150×50 nm, 210×70 nm, and 240×80 nm, with corresponding $\Delta = 42$, 63, and 74, respectively. The easy magnetization axes for the free and polarizing layers are collinear in the film plane, and the free layers in all devices have significant perpendicular

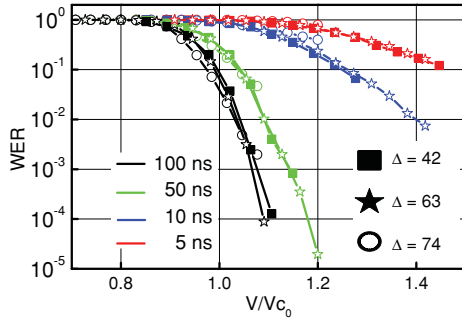


FIG. 1. (Color online) Experimental WER results for three different devices at different pulse durations. The measured V_{c0} are approximately 0.25, 0.28, and 0.32 V for devices with $\Delta = 42$, 63, and 74, respectively.

anisotropy ($\approx 80\%$ of M_s). Our test procedure is as follows: We set the device state to the high (low) resistance state with a reset pulse, record the initial state with a small read signal, apply a write pulse, and record the device state after the write pulse. The procedure is repeated 10^6 times to acquire enough statistical data to reliably determine the switching probability (P_{sw}). We performed both high-to-low and low-to-high resistance switching, which show qualitatively similar behavior, and we present here only the data for high-to-low resistance switching.

Figure 1 shows the WER ($WER = 1 - P_{sw}$), as a function of the write voltage amplitude for several different pulse durations. It can be seen that all devices, regardless of size, show similar behavior when plotted on a normalized voltage scale (V/V_{c0}). At long pulse widths (≥ 50 ns), the WER decreases sharply (has a large slope), and the voltage needed to achieve WER less than 10^{-5} , for example, is only slightly above V_{c0} , which is in agreement with the recent results.¹⁰ All WER at long times (100 ns-1 μ s) have roughly the same slope. However, at shorter times (≤ 10 ns) the WER falls off more slowly with increasing voltage (has smaller slope), and the voltage needed to achieve a WER of 10^{-5} is significantly higher (extrapolation gives $\approx 1.85V_{c0}$ at 10 ns and $\approx 2.7V_{c0}$ at 5 ns). This general behavior appears in all of the tens of devices we tested, and presents a significant problem for STT-RAM devices that need to operate at write times of ≈ 10 ns since reliable switching would require applied voltages that are a significant fraction of V_{bd} . In a minority of devices, we also observed nonsingle-exponential decay of the WER (not shown here) that was recently reported in Ref. 11, and further exacerbates the issue. Here, we focus only on the parameters that affect the WER in devices that have a well-defined single-exponential decrease of the WER with voltage/current.

III. MACROSPIN SIMULATIONS

To better understand the switching behavior in these devices, the origin of the WER, and the methods to improve the WER, we performed numerical simulations of spin-torque-induced switching by use of a macrospin model with finite temperature²¹ with the following parameters: $\mu_0 M_s = 1$ T, $\alpha = 0.01$, $T = 300$ K, $\mu_0 H_{ext} = 0$ T (no external field),

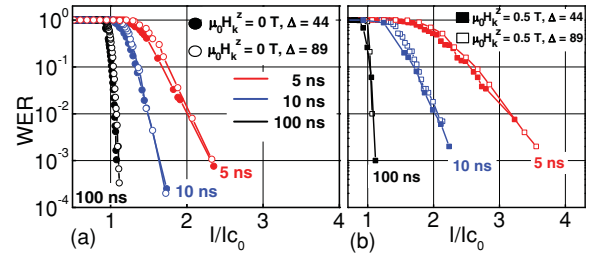


FIG. 2. (Color online) WER simulation data for devices with: (a) $\Delta = 44$, $I_{c0} = 0.34$ mA (filled circles) and $\Delta = 89$, $I_{c0} = 0.58$ mA (open circles) and $\mu_0 H_k^z = 0$ T; (b) $\Delta = 44$, $I_{c0} = 0.16$ mA (filled squares) and $\Delta = 89$, $I_{c0} = 0.28$ mA (open squares) and $\mu_0 H_k^z = 0.5$ T.

$P = 0.8$ (polarization of spin injection current), and $\Lambda = 1$ (spin-torque asymmetry). The field-like torque term and the Ohmic heating were not included in the simulations. At each value of the injected current, the switching probability was determined with up to 3×10^5 switching trials.²² The simulated structures have dimensions $150 \times 50 \times 2$ nm, and $250 \times 50 \times 2$ nm, with $\Delta = 44$ and 89, respectively. Figure 2(a) shows the WER for two different devices simulated without any perpendicular anisotropy ($\mu_0 H_k^z = 0$ T) at 5, 10, and 100 ns. Although micromagnetic simulations are needed to fully describe the switching process, we find that the macrospin model qualitatively reproduces the results shown in Fig. 1. The simulations show a simple exponential decrease of the WER (the linear region on the semilogarithmic plots) and qualitatively agree with the experimental data shown in Fig. 1 insofar as the WER slope decreases with decreasing pulse time. We see that when plotted on a normalized current scale (I/I_{c0}) the WER does not depend on Δ , which agrees with recent theoretical predictions²³ and with our data.

In Fig. 2(b), we have included the results of simulations with perpendicular anisotropy $\mu_0 H_k^z = 0.5$ T ($H_k^z < H_k^d$). At long times (≥ 100 ns), the $H_k^z > 0$ does not strongly influence the WER when plotted on the normalized current scale (I/I_{c0}), but at shorter times (≤ 10 ns) the nonzero H_k^z slightly increases the WER for a given I/I_{c0} . However, H_k^z also affects I_{c0} , and to directly compare the effect of nonzero H_k^z , we plot in Fig. 3(a) the WER versus absolute current I at 5 ns with $\mu_0 H_k^z = 0$ T and $\mu_0 H_k^z = 0.5$ T for a device with $\Delta = 44$. Here, we see that the effect of H_k^z is to shift the WER knee to lower absolute currents, keeping the same slope, thus decreasing the WER at a given current. In the extreme case that the H_k^z were increased to the point where the WER slope intersects the current axis at $I = 0$ mA [dashed blue line in Fig. 3(a)], then a current required for the WER of 10^{-4} , for example, would be reduced by roughly 50% compared to the case with $\mu_0 H_k^z = 0$ T. While such a device would not be technically viable, this does show the ultimate limit of how much the WER can be reduced by increasing H_k^z with the given simulation parameters.

A similar reduction of the WER, at a given current, can be achieved by a reduction of α as illustrated in Fig. 3(c). By comparing Figs. 3(a) and 3(c), we can see that the WER slope is not a function of H_k^z and α , indicating that the dashed line represents a robust limit to the absolute WER. The plot

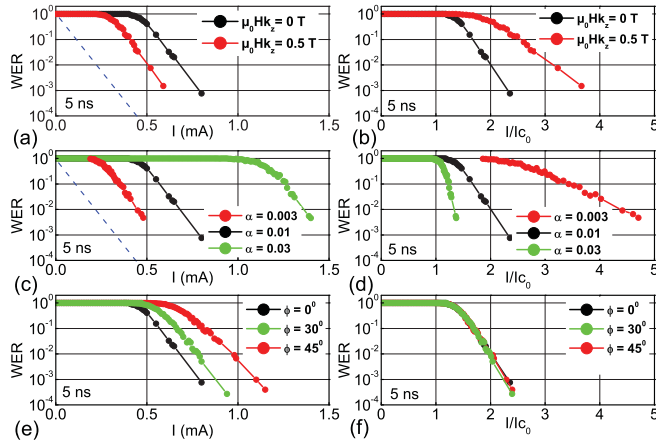


FIG. 3. (Color online) WER simulation data for a device with $\Delta = 44$ at 5-ns pulse duration: (a,b) with $\mu_0 H_k^z = 0$ T and $\mu_0 H_k^z = 0.5$ T; (c,d) with different α at $\mu_0 H_k^z = 0$ T; (e,f) at different angles ϕ at $\mu_0 H_k^z = 0$ T. The WER data are plotted vs. I in (a), (c), and (e) and vs. normalized current I/I_{c0} in (b), (d), (f).

of the WER as a function of I/I_{c0} in Fig. 3(d) gives the impression that the WER becomes worse for lower α , which is incorrect because I_{c0} also decreases with decreasing α . Thus, while plotting the WER on a normalized scale (I/I_{c0}) does allow for direct comparison with theoretical predictions, doing so can be also be misleading when comparing the effects of device parameters on the absolute WER.

IV. DISCUSSION

As the behavior of the WER shown in Fig. 1 is qualitatively reproduced by the macrospin model, this indicates that the explanation of the increase in the WER at short times lies in the basic underlying physics of spin-torque switching and the thermal effects, while other effects such as micromagnetics and device imperfections likely play a secondary role. The cause of the WER increase appears to be associated with a “stagnation point” or “zero-torque point”^{24,25} on the switching trajectory where the spin polarization is parallel to the free layer magnetization, so that the spin-torque vanishes. Thermal fluctuations influence the switching process both by creating a distribution of initial states at the onset of the pulse and by inducing fluctuations during the switching process. The distribution of initial states can include the stagnation point leading to the WER, or thermal fluctuations during the switching process can cause the switching trajectory to diffuse back to the stagnation point, so that the energy in the system is essentially dissipated. Once the energy is lost, the magnetization might not have enough time to build up the oscillations again and would fail to switch.

One potential way to test the influence of the distribution of initial states on the WER is to rotate the angle between the fixed and free layers. In Fig. 3(e), we plot the WER as a function of the in-plane offset angle of the polarization with respect to the free-layer easy axis, which only increases the WER. By comparing Figs. 3(a), 3(c), and 3(e), we see that the noncollinear orientation is detrimental because it increases I_{c0} (Ref. 26), and does not strongly affect the slope of the WER.

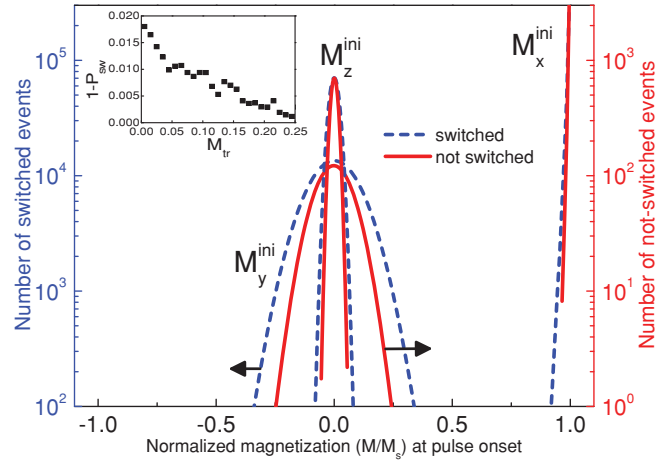


FIG. 4. (Color online) Distribution of magnetization components at the pulse onset for switched and not-switched events. Inset: probability of not-switching vs. transverse magnetization M_{tr} .

For completeness, we also plot the same data on a normalized scale (I/I_{c0}) in Fig. 3(f). Here, the WER, as a function of I/I_{c0} , is not dependent on ϕ . We also simulated the case where the spin current polarization is tilted out of the film plane by $\theta = 5^\circ - 30^\circ$ (not shown), in which case the WER considerably increases, because the free layer magnetization can start to oscillate around the out-of-plane axis. Our simulations also show that the above-mentioned parameters improve the WER only to some extent by decreasing the intrinsic switching voltage, and not by increasing the WER slope which would be more desirable. The lack of improvement when the angle of the polarization layer is rotated with respect to the free layer axis suggests that the thermal effects during the switching play an important role in determining the WER and that the magnitude of the spin torque at onset alone is less significant.

To look at this in a different way, in Fig. 4 we plot the distribution of the initial magnetization states at the pulse onset for each of the 3×10^5 simulated switching attempts, of which there were about 3000 not-switched events. The data correspond to the point in Fig. 2(a) having $\mu_0 H_k^z = 0$ T, $\Delta = 44$, $I/I_{c0} = 2$, WER = 0.01, and 5-ns pulse duration. Interestingly, the distributions of the components of the initial transverse magnetization states (M_y^{ini} and M_z^{ini}) for switched and not-switched events overlap. This shows that the not-switched events do not simply correspond to a specific subset of initial magnetization states, but that the stochastic thermal fluctuations occurring during the switching process also play a significant role.

This is supported by the plot of the probability of not-switching versus the transverse magnetization [$M_{tr} = \sqrt{(M_y^{\text{ini}})^2 + (M_z^{\text{ini}})^2}$] at the pulse onset shown in the inset of Fig. 4. While the highest probability of not-switched events does correspond to the lowest values of M_{tr} , the plot also shows that starting with an initial transverse magnetization $M_{tr} > 0$ is also important in determining the WER. This indicates that the initial magnetization conditions alone do not determine the WER, and that the fluctuations occurring during the switching process are as important in determining whether or not the device will switch.

V. SUMMARY

In summary, we have found experimentally that the physics of spin-torque switching sets limitations on how efficiently the switching can be performed at time scales less than 50 ns. This implies that write voltages/currents must be several times larger than the nominal critical value to obtain reliable switching with low WER at these time scales. The same qualitative behavior is also seen in macrospin simulations, indicating that this is a fundamental problem with the simple STT-RAM structure. Simulations show that the WER can be reduced to some extent by the use of materials with perpendicular anisotropy and low damping. The WER is

caused by a combination of initial starting states that include the stagnation point and thermal diffusion back to those states during the switching process, which cannot be counteracted by simply offsetting the angle of spin polarization from the magnetic easy axis.

ACKNOWLEDGMENTS

The authors acknowledge support by OMP, ARRA, and DARPA. The authors also thank Dr. Jürgen Langer of the Singulus Technologies AG for providing the wafers with the starting thin-film stack. This work is supported by U.S. Government, and is not subject to U.S. copyright.

*heindl@nist.gov

¹J. C. Slonczewski, *J. Magn. Magn. Mater.* **159**, L1 (1996).

²L. Berger, *Phys. Rev. B* **54**, 9353 (1996).

³J. A. Katine and E. E. Fullerton, *J. Magn. Magn. Mater.* **320**, 1217 (2008).

⁴S. Ikeda, J. Hayakawa, Y. M. Lee, F. Matsukura, Y. Ohno, T. Hanyu, and H. Ohno, *IEEE Trans. Electron Devices* **54**, 991 (2007).

⁵S. Ikeda, K. Miura, H. Yamamoto, K. Mizunuma, H. D. Gan, M. Endo, S. Kanai, J. Hayakawa, F. Matsukura, and H. Ohno, *Nat. Mater.* **9**, 721 (2010).

⁶D. C. Worledge, G. Hu, D. W. Abraham, J. Z. Sun, P. L. Trouilloud, J. Nowak, S. Brown, M. C. Gaidis, E. J. O'Sullivan, and R. P. Robertazzi, *Appl. Phys. Lett.* **98**, 022501 (2011).

⁷E. Chen, D. Apalkov, Z. Diao, A. Driskill-Smith, D. Druist, D. Lottis, V. Nikitin, X. Tang, S. Watts, S. Wang, S. A. Wolf, A. W. Ghosh, J. W. Lu, S. J. Poon, M. Stan, W. H. Butler, S. Gupta, C. K. A. Mewes, T. Mewes, and P. B. Visscher, *IEEE Trans. Magn.* **46**, 1873 (2010).

⁸K. Lee and S. Kang, *IEEE Trans. Magn.* **46**, 1537 (2010).

⁹ $V(I)$ is the applied switching voltage (current) at $T = 300$ K and $V_{c_0}(I_{c_0})$ is the intrinsic long-time switching voltage (current) at $T = 0$ K. While the actual experimental measurements were performed using voltage pulses of different amplitude, in simulations we use current pulses since, in the simple model of spin transfer, the current is more directly related to the current induced torque. V_{c_0} is experimentally determined using “read disturb” and “pulse-width dependence of switching probability” techniques, while I_{c_0} in the simulations was determined by extrapolating switching currents to $T = 0$ K and infinite switching time.

¹⁰L. Z. Diao, Z. S. Wang, Y. Ding, A. Panchula, E. Chen, L.-C. Wang, and Y. Huai, *J. Phys. Condens. Matter* **19**, 5209 (2007).

¹¹T. Min, Q. Chen, R. Beach, G. Jan, C. Horng, W. Kula, T. Torng, R. Tong, T. Zhong, D. Tang, P. Wang, M.-M. Chen, J. Z. Sun, J. K. DeBrosse, D. C. Worledge, T. M. Maffitt, and W. J. Gallagher, *IEEE Trans. Magn.* **46**, 2322 (2010).

¹²D. C. Worledge, in *2010 IEEE International Electron Devices Meeting* (2010).

¹³M. Schäfers, V. Drewello, G. Reiss, A. Thomas, K. Thiel, G. Eilers, M. Münzenberg, H. Schuhmann, and M. Seibt, *Appl. Phys. Lett.* **95**, 232119 (2009).

¹⁴A. A. Khan, J. Schmalhorst, A. Thomas, O. Schebaum, and G. Reiss, *J. Appl. Phys.* **103**, 123705 (2008).

¹⁵Q. Chen, T. Min, T. Torng, C. Horng, D. Tang, and P. Wang, *J. Appl. Phys.* **105**, 07C931 (2009).

¹⁶ E_{barrier} is the switching energy barrier, which depends on the free-layer in-plane anisotropy H_k^x and the magnetization M_s , k_B is Boltzmanns constant, and T is the device temperature.

¹⁷J. Z. Sun, *Phys. Rev. B* **62**, 570 (2000).

¹⁸L. Liu, T. Moriyama, D. C. Ralph, and R. A. Buhrman, *Appl. Phys. Lett.* **94**, 122508 (2009).

¹⁹The details of the experimental setup will be published elsewhere. The pulse rise time was ≈ 100 ps.

²⁰Wafers with starting thin film stack were prepared by Singulus Technologies Inc, [<http://www.singulus.de/en.html>]. The ion milling was stopped at the MgO barrier, meaning that only the free ferromagnetic layer is patterned. Wafer level current-in-plane-tunneling (CIPT) measurements and measurements on processed devices give resistance-area (RA) products of $3 \Omega\mu\text{m}^2$ and tunneling magnetoresistance (TMR) ratios of about 60%. The devices have elliptical shapes with an aspect ratio of 3 to 1 and sizes ranging from 50×150 nm to 80×240 nm. For the device with $\Delta = 42$, the average resistance is $R \approx 510 \Omega$. Devices from other wafers with RA products ranging up to $25 \Omega\mu\text{m}^2$, with various sizes, compositions, and thermal stability factors also are in agreement with the conclusions presented here.

²¹S. E. Russek, S. Kaka, W. H. Rippard, M. R. Pufall, and T. J. Silva, *Phys. Rev. B* **71**, 104425 (2005).

²²All simulations start after a 10-ns wait time to allow the system to reach the equilibrium. Pulse rise and fall times are 100 ps.

²³W. H. Butler, in *Proceedings of the 55th MMM Conference, Atlanta* (2010).

²⁴T. Devolder, C. Chappert, and K. Ito, *Phys. Rev. B* **75**, 224430 (2007).

²⁵K. Roy, S. Bandyopadhyay, and J. Atulasimha, e-print [arXiv:1012.0819v1](https://arxiv.org/abs/1012.0819v1).

²⁶F. B. Mancoff, R. W. Dave, N. D. Rizzo, T. C. Eschrich, B. N. Engel, and S. Tehrani, *Appl. Phys. Lett.* **83**, 1596 (2003).